The sensitivity of estuarine aragonite saturation state and pH to the carbonate chemistry of a freshet-dominated river

Benjamin L. Moore-Maley[1], Debby Ianson[1,2], and Susan E. Allen[1]

[1]Department of Earth, Ocean and Atmospheric Sciences, University of British Columbia, Vancouver, British Columbia, Canada

[2]Fisheries and Oceans Canada, Institute of Ocean Sciences, Sidney, British Columbia, Canada

Correspondence to: Benjamin Moore-Maley (bmoorema@eoas.ubc.ca)

Abstract.

Ocean acidification threatens to reduce pH and aragonite saturation state (Ω_A) in estuaries, potentially damaging their ecosystems. However, the impact of highly variable river total alkalinity (TA) and dissolved inorganic carbon (DIC) on pH and Ω_A in these estuaries is unknown. We assess the sensitivity of estuarine surface pH and Ω_A to river TA and DIC using a coupled biogeochemical model of the Strait of Georgia on the Canadian Pacific coast and place the results in the context of global rivers. The productive Strait of Georgia estuary has a large, seasonally variable freshwater input from the glacially fed, undammed Fraser River. Analyzing TA observations from this river plume and pH from the river mouth, we find that the Fraser is moderately alkaline (TA 500–1000 μmol kg^{-1}) but relatively DIC-rich. Model results show that estuarine pH and Ω_A are sensitive to freshwater DIC and TA, but do not vary in synchrony except at high DIC:TA. The asynchrony occurs because increased freshwater TA is associated with increased DIC, which contributes to an increased estuarine DIC:TA and reduces pH, while the resulting higher carbonate ion concentration causes an increase in estuarine Ω_A. When freshwater DIC:TA increases (beyond $\sim$1.1), the shifting chemistry causes a paucity of the carbonate ion that overwhelms the simple dilution/enhancement effect. At this high DIC:TA ratio, estuarine sensitivity to river chemistry increases overall. Furthermore, this increased sensitivity extends to reduced flow regimes that are expected in future. Modulating these negative impacts is the seasonal productivity in the estuary which draws down DIC and reduces the sensitivity of estuarine pH to increasing DIC during the summer season.

1 Introduction

Estuaries support productive ecosystems (Cloern et al., 2014) and significant human populations (Cloern et al., 2015). Critical trophic links within many of these ecosystems may be negatively impacted by increases in dissolved inorganic carbon (DIC) and reduced pH associated with ocean acidification (Haigh et al., 2015). Those organisms using the calcium-carbonate mineral form aragonite in their external hard parts (e.g., some Molluscs) are especially vulnerable since oceanic CO$_2$ uptake lowers the aragonite saturation state (Ω_A) of seawater (Waldbusser et al., 2015). While carbonate system dynamics and/or acid-base chemistry have been studied extensively in marine (e.g., Jiang et al., 2015) and freshwater (e.g., Schindler, 1988) environments, less is known in the diverse estuaries where these two zones meet (Salisbury et al., 2008; Hagens and Middelburg, 2016; Cai et al., 2017).

Estuarine systems are complex, cover large salinity ranges that challenge current measurement techniques and are generally under-sampled (Ianson et al., 2016; Cai et al., 2017). The carbonate chemistry in the rivers that feed these estuaries may also be exceptionally variable (Cai et al., 1998), ranging from rivers with low DIC to total alkalinity (DIC:TA) ratios and high pH (> 8) like the Mississippi River (Hu and Cai, 2013) to blackwater rivers that have low pH (< 5) (Cai et al., 1998; de Fátima F. L. Rasera et al., 2013). Along a salinity gradient there may exist maximum sensitivity zones that are especially vulnerable to acidification. The strength and location of these zones depend on the river endmember carbonate chemistry (Hofmann et al., 2009; Hu and Cai, 2013; Xue et al., 2017). This sensitivity is generally expected to increase as the ocean absorbs CO_2 and becomes warmer (Hagens and Middelburg, 2016).

In addition, seasonality is often strong and single rivers and estuaries may experience highly variable conditions in space and time (Hellings et al., 2001; de Fátima F. L. Rasera et al., 2013; Waldbusser and Salisbury, 2014; Hunt et al., 2014; Voss et al., 2014; Ianson et al., 2016; Xue et al., 2017). Carbonate and silicate weathering are major sources of river DIC and TA in most rivers (Meybeck, 1987; Amiotte Suchet et al., 2003). Carbonates are concentrated globally in the northern mid-latitudes (Amiotte Suchet et al., 2003), and several carbonate-rich, mid-latitude watersheds demonstrate high TA and large TA flow-dependence such as the Changjiang and Mississippi Rivers (Cai et al., 2008). TA flow-dependence is also common among low-TA, low-latitude rivers like the Amazon (Richey et al., 1990) and Congo (Wang et al., 2013) Rivers, although organic carbon contributions can complicate this behavior. In the Congo River for example, TA is flow-dependent but DIC is persistently high year-round (Wang et al., 2013). On top of natural variability, many estuaries also experience heavy anthropogenic pressure (Frankignoulle et al., 1996; Zhai et al., 2007; Cai et al., 2017), making them particularly vulnerable to ocean acidification (Cai et al., 2011, 2017) and in some cases the subject of intensive management and policy initiatives (Fennel et al., 2013).

In the present study, we determine the sensitivity of Ω_A and pH in a large, mid-latitude, fjord estuary (Strait of Georgia, Canada) to changes in freshwater TA and DIC using a quasi one-dimensional biogeochemical model. This model mechanistically parameterizes horizontal two-dimensional estuarine flow as a function of river flow. Few carbonate data exist in the river plume region and fewer still at the river mouth, motivating us to perform these broad analyses. We establish a freshwater TA range and flow dependent variability for the system by extrapolating TA observations from the Fraser River plume region to zero salinity. We use autonomous pH measurements from an Environment and Climate Change Canada (ECCC) mooring near the Fraser River mouth with our estimated TA to constrain freshwater DIC, since we lack reliable direct DIC observations in the Fraser River. From the model estuarine Ω_A and pH results across 18 river chemistry scenarios and 12 recent hydrological annual cycles, we identify regions of the freshwater carbonate chemistry range, expressed as both DIC:TA and DIC-TA, that produce enhanced estuarine pH and Ω_A sensitivity to this freshwater chemistry. We characterize these regions in terms of (past) low DIC and (future) high DIC freshwater carbonate chemistry and show how conditions in this temperate estuary deviate from theoretical mixing curves due to the strong local seasonal biological cycles. We further discuss the implications of these results for future climate with emphasis on the anticipated changes in hydrological cycles.

2 Methods

2.1 Study area

The Strait of Georgia (Fig. 1) is a large ($\sim$6800 km^2, $>$400 m deep), temperate, semi-enclosed, fjord-like estuarine sea with strong seasonal stratification, productivity, and carbonate chemistry cycles (Moore-Maley et al., 2016; Ianson et al., 2016). This high productivity supports abundant populations of shellfish, finfish, and other higher organisms that may be sensitive to pH and Ω_A anomalies (Haigh et al., 2015). The Fraser River, the primary freshwater source, drains approximately 238,000 km^2 with seasonally variable discharge ($\sim$800 to 12,000 m^3 s^{-1} at Hope, ECCC data, http://wateroffice.ec.gc.ca) due to summer snow/ice melt and lack of dams throughout most of the watershed. This large freshwater flux is partially contained by narrow passages and tidal mixing over sills (Pawlowicz et al., 2007), and thus imparts a significant freshwater influence on the Strait especially compared with regions where large rivers meet the ocean directly such as the nearby Columbia River plume region (Roegner et al., 2011). These same coastal and topographic features create long residence times, causing carbon to accumulate and making the Strait DIC-rich relative to the open ocean (Ianson et al., 2016) despite a strong, seasonal DIC upwelling signal over the outer shelf (Bianucci et al., 2011). The large freshwater footprint, together with the abundance of previous circulation (e.g., LeBlond, 1983; Pawlowicz et al., 2007), ecology (e.g., Masson and Peña, 2009; Allen and Wolfe, 2013), and acidification studies (e.g., Moore-Maley et al., 2016; Ianson et al., 2016) make the Strait an ideal system for investigating the response of pH and Ω_A to freshwater carbonate chemistry in a complicated estuarine setting.

The seasonal progression of productivity in the Strait of Georgia begins with a characteristic spring phytoplankton bloom (Allen and Wolfe, 2013) followed by a shallow ($\sim$20 m) surface layer of productivity throughout the summer that transitions into weaker fall blooms before returning to the background winter state (Harrison et al., 1983). Below this productive surface layer, the DIC-rich intermediate basin is persistently aragonite undersaturated. This signal is mixed to the surface throughout winter, but summer productivity maintains high pH and aragonite supersaturation in the top 20 m of the water column (Ianson et al., 2016). The strength and timing of this seasonal DIC cycle is strongly linked to local wind, irradiance, and freshwater forcing, the latter of which maintains the strongest influence of the three during summer (Moore-Maley et al., 2016).

The Fraser River watershed spans four distinct geologic belts (Fig. 1a) that transition from the carbonate-rich Foreland Belt to the silicate-rich Coast Belt (Cameron and Hattori, 1997). Carbonate and silicate weathering thus dominate the watershed (Voss et al., 2014); carbonate weathering generally produces TA faster than silicate weathering (Meybeck, 1987). Observed Fraser River TA varies strongly throughout the watershed, but generally accumulates along the Foreland Belt, decreases along the Coast Belt, and is highest at low flow stage (Voss et al., 2014). Fraser River TA thus appears to be produced primarily by carbonate weathering in the upper watershed, diluted by low-TA seaward tributaries, and flow dependent. There are no data in the Fraser River region to date that determine organic acids and bases that may contribute significantly to TA, as they do in some coastal areas (Cai et al., 1998; Koeve and Oschlies, 2012; Kim and Lee, 2009; Hernández-Ayón et al., 2007) and rivers (Hunt et al., 2011; Kennedy, 1965). Carbonate alkalinity is estimated to be as low as 10% of TA in the Congo (Wang et al., 2013) and Kennebec Rivers (Hunt et al., 2014).

2.2 Model

2.2.1 Overview

In order to resolve the primary productivity in the strongly stratified Strait of Georgia, it is necessary to have fine vertical resolution but it is not necessary to model the whole water column. Given the summer depth of the chlorophyll maximum of 5 m (Peña et al., 2016) and typical mixing layer depths of 1-7 m (Collins et al., 2009), we use 0.5 m vertical resolution and model the upper 40 m. The vertical model is located directly to the northwest of the Fraser River plume region (Fig 1b). The region of the Fraser plume is dominated by estuarine circulation and wind-mixing. The dynamics have been well-studied (e.g., Pawlowicz et al., 2007) giving us the information to effectively parameterize higher dimensional processes with a one dimensional (1-D) model (Collins et al., 2009; Allen and Wolfe, 2013). The benefits of a 1-D model are the quick run times that allow us to simulate many parameter variations over multiple annual cycles (Moore-Maley et al., 2016).

Accurately simulating mixing of the stratified plume with the waters below is required to reproduce the biology and chemistry of the plume. To this end, the physical model is based on the KPP mixing-layer model which includes the impacts of winds and heat/cooling on currents and mixing (Large et al., 1994). We add baroclinic pressure gradients and estuarine circulation to the model. More specifically, we add (1) freshwater and freshwater tracers to the mixing layer of the model, (2) a vertical upwelling due to entrainment and (3) a seaward advective loss to conserve volume flux. All three are defined in terms of the total freshwater discharge from the Fraser River and other small rivers (Collins et al., 2009).

The model represents a column of water with radius about one tidal excursion. It uses a 15 minute timestep. We explicitly model *in situ* temperature, ITS-90 (Preston-Thomas, 1990), and practical salinity, PSS-78 (UNESCO, 1981), as physical state variables.

The biological model contains three nutrient classes (nitrate, ammonium, dissolved silica), three photosynthesizer classes (diatoms, mixotrophs as *Mesodinium rubrum*, nanoflagellates), three grazer classes (*M. rubrum*, microzooplankton, mesozooplankton), and three detritus classes (dissolved and particulate organic nitrogen, biogenic silica). *M. rubrum* (a ciliated protozoan) retains functional chloroplasts during grazing and uses them to perform photosynthesis. Calcifying phytoplankton (e.g., coccolithophores) are assumed to contribute minimally to productivity in the Strait of Georgia (Haigh et al., 2015) and were absent from satellite observations in the Strait prior to 2016 (J. Gower, personal communication, 2014; NASA Earth Observatory, http://earthobservatory.nasa.gov/IOTD/view.php?id=88687) – they are not explicitly modeled.

DIC and TA are both explicitly modeled and are coupled to the biological growth and remineralization cycles (Moore-Maley et al., 2016). Transfer of CO_2 across the air-sea interface in the surface grid cell is parametrized according to Fick's second law of diffusion (Sarmiento and Gruber, 2006), using gas transfer coefficient (Nightingale et al., 2000), Schmidt number (Wanninkhof, 1992), and K_0 solubility coefficient (Weiss, 1974) parameterizations. Model pH (total scale) and Ω_A are calculated from model DIC, TA, dissolved silica, temperature, salinity, pressure, and estimated phosphate using the CO2SYS program (Lewis and Wallace, 1998) and full salinity range K_1 and K_2 constants (Millero, 2010). Phosphate is roughly approximated (± 1 μmol kg^{-1}, Riche (2011)) from model nitrate using the Redfield N:P ratio. Calcium ion concentrations, required for Ω_A

calculation, are approximated by a linear regression to salinity (Riley and Tongudai, 1967), and by the mean observed calcium ion concentration near the Fraser River mouth, 350 μmol kg^{-1} (Voss et al., 2014), where salinity < 1.

2.2.2 Initialization and forcing

We use profiles of temperature, salinity, fluorescence, chlorophyll a, nitrate, and dissolved silica (1999 through 2012) measured near the model site (Pawlowicz et al., 2007; Masson, 2006; Masson and Peña, 2009; Peña et al., 2016) (D. Masson, personal communication, 2014) to initialize the model (see Moore-Maley et al., 2016). Model runs are initialized in autumn and run through a full year and then beyond until the end of the following December. Our analysis starts at the beginning of the year following the initialization date which is always a longer period than the 30-day spin-up period. Initial phytoplankton, zooplankton, and detritus concentrations are determined according to Moore-Maley et al. (2016). Since few DIC and TA data are available, we use a representative fall profile (11 September, 2011 (Ianson et al., 2016)) to initialize model DIC and TA. Model pH and Ω_A are not sensitive to initial carbonate chemistry conditions after the spin-up period. Time-averages (fluorescence, chlorophyll a, nitrate, dissolved silica) and annual fits (temperature, salinity, DIC, TA) of the initialization data near 40 m are used to set the 40 m boundary conditions (Moore-Maley et al., 2016). Average model 40 m boundary conditions are summarized as the model seawater endmember in Table 1.

The model is forced at the surface (Allen and Wolfe, 2013) by wind stress calculated from hourly wind speed and direction observed at Sandheads weatherstation, and by heat fluxes derived from cloud fraction, air temperature and relative humidity observed at Vancouver International Airport (Fig. 1b; ECCC observations, http://climate.weather.gc.ca/). Total freshwater flux (volume/time) into the Strait of Georgia is prescribed (Allen and Wolfe, 2013) using daily river discharge measurements obtained by ECCC (http://www.wateroffice.ec.gc.ca/) in the Fraser River at Hope and in the Englishman River at Parksville (Fig. 1b). Englishman River discharge is used in this study as a proxy for the contribution of small, rainfall-dominated rivers to the freshwater budget of the Strait (Collins et al., 2009). Heat and nutrient fluxes due to freshwater are prescribed (Moore-Maley et al., 2016) as concentration × flux. Model freshwater endmember concentrations are summarized in Table 1.

2.2.3 Evaluation

Previous studies using the model have evaluated it against physical, biological and chemical data. The vertical profiles of density and in particular, the depth of the halocline are well represented (Collins et al., 2009). The model captures interannual variability in the biology and in the physics driving the biological variability – the model accurately predicts the timing of the spring phytoplankton bloom (Allen and Wolfe, 2013; Allen et al., 2016). The large seasonal variation of the carbon cycle is captured with some underestimation of DIC in the summer due to over-productivity (Moore-Maley et al., 2016), a common problem with coupled models in the Strait of Georgia (e.g., Peña et al., 2016). Evaluation of pH and Ω_A in the model shows both systematic and non-systematic errors (Moore-Maley et al., 2016). The variations in pH observations are well captured by the model with a correlation coefficient of 0.80. There is a positive bias which is higher at high pH. The root-mean-squared error (RMSE) for pH is 0.16 but removing the systematic error (by fitting a line between the model and observations) gives a non-systematic or scatter RMSE of 0.06. One-third of this discrepancy can be explained by mismatches between model time

and space. The evaluation is similar for Ω_A, correlation of 0.79, a RMSE of 0.51 with a scatter RMSE of 0.18, and average mismatches due to time and space of 0.05. Thus, the non-systematic error is sufficiently small to support the model's use for the process studies described here. Note that the systematic bias means that the model is conservative, over-predicting both pH and Ω_A.

2.3 Sensitivity analysis

In order to test the sensitivity of the biogeochemical model to changes in freshwater chemistry, we select ranges of freshwater TA and DIC endmembers based on observed TA in the Fraser plume and pH near the Fraser River mouth. We extrapolate estuarine TA data (Ianson et al. (2016), Table S1) sampled throughout the water column, following modern sampling and analysis procedures (Dickson et al., 2007), from seven recent (2010–2016) sampling campaigns near the Fraser River plume (Fig. 1b) to zero salinity using linear regression in order to establish freshwater TA endmembers across multiple seasons (Fig. 2a). We only consider profiles that include at least one TA sample below a salinity of 20 to allow sufficient river influence.

DIC can vary at constant pH, however DIC:TA cannot (given constant temperature and salinity). Thus rather than prescribing freshwater DIC directly, we define freshwater DIC:TA endmembers based on observations from the ECCC Fraser River Water Quality Buoy (Fig. S1) moored approximately 10 km upstream of the river mouth (Fig. 1b). Buoy pH was measured potentiometrically using a regularly-inspected (bimonthly to monthly), hull-mounted, YSI ADV6600 multisensor and recorded hourly from 2008 until present (Ethier and Bedard, 2007). We calculate DIC:TA from buoy pH using the CO2SYS program (Lewis and Wallace, 1998) and full salinity range K_1 and K_2 constants (Millero, 2010).

There are uncertainties associated with the extrapolated freshwater TA endmembers due to our assumptions that TA is conservative across such a wide salinity range and that organic alkalinity contributions in the Fraser Plume region are small. There are also significant uncertainties in the freshwater pH observations given that potentiometric pH measurements in freshwater are generally no more precise than 0.2 units (Covington et al., 1983). A thorough error analysis of these data is intractable given the paucity of data and our lack of additional parameters such as $p\mathrm{CO}_2$. Instead, given these uncertainties, we consider the extrapolated freshwater TA endmembers and the freshwater DIC:TA endmembers calculated from the buoy pH record to represent approximate seasonal ranges of freshwater carbonate chemistry rather than absolute values.

The freshwater TA endmembers span an approximate range between 500 and 1000 μmol kg^{-1} (Fig. 2). We thus define five constant freshwater TA (hereinafter TA$_f$) scenarios: three at the minimum, center and maximum of the extrapolated endmember range (500, 750 and 1000 μmol kg^{-1}, respectively) and two more to represent extremes beyond our estimated range at 250 and 1250 μmol kg^{-1} (Table 2). The extrapolated endmembers also vary seasonally, demonstrating significant hysteresis with respect to Fraser River discharge at Hope (lowpass filtered with a 40-day cutoff, Q_{filt}, Fig. 2b) and a positive correlation to dQ_{filt}/dt (Fig. 2c). We thus add an additional flow dependent TA$_f$ scenario based on a linear regression of the extrapolated TA endmembers to dQ_{filt}/dt given by

$$\mathrm{TA}_f = \frac{\mathrm{TA}_0 t_0}{Q_0}\frac{dQ_{filt}}{dt} + \mathrm{TA}_0 \tag{1}$$

where $TA_0 = 750$ μmol kg^{-1}, $Q_0 = 840$ m^3 s^{-1} and $t_0 = 86400$ s (Table 2). This flow dependent TA_f converges to TA_0 when $dQ_{filt}/dt = 0$ and increases or decreases when dQ_{filt}/dt becomes either positive or negative (e.g., Fig. 2c).

Buoy pH is seasonally variable (Fig. S1) and changes are likely driven primarily by biological productivity since the correlation to river discharge is weak and summer river warming would tend to drive pH seasonal cycles in the opposite direction. The complete buoy pH record follows a Gaussian distribution with a median of approximately 7.5 and first and 99th percentiles at approximately 7.1 and 7.9, respectively (Fig. S1). Over the annual model freshwater temperature range (2.5-19.3°C) these pH values, in order from highest to lowest, correspond to average DIC:TA values of 1.032, 1.089, and 1.226. We use these freshwater DIC:TA values (hereinafter DIC_f:TA_f) as our respective Low Carbon, Med Carbon, and High Carbon freshwater endmember cases (Table 2). The Low Carbon case is typical of present-day high TA rivers with low DIC:TA such as the Mississippi (Cai, 2003) and Changjiang (Zhai et al., 2007) Rivers. We suggest that this scenario represents a lower limit in the Fraser River and may represent past chemistry (lower pCO$_2$). Likewise, we consider the High Carbon case to represent possible future pCO$_2$ increases but still within the range of present-day Fraser River pH observations (buoy pH). This High Carbon scenario still has a lower DIC_f:TA_f than low pH, weakly-buffered rivers such as the Kennebec (Hunt et al., 2014) and Congo (Wang et al., 2013) Rivers. These three DIC_f:TA_f cases combined with our six TA_f cases produce 18 individual river endmember chemistry scenarios that we use in the biogeochemical model (summarized in Table 2).

For each permutation of TA_f and DIC_f:TA_f, we ran the model over the same 12-year period (2001–2012) used in previous studies involving this model (e.g., Moore-Maley et al., 2016) to maintain consistency with previous work and to ensure a wide range of climatological forcing regimes. With 18 possible combinations of TA_f and DIC_f:TA_f, we ran the model a total of 216 times. Since the seasonality of DIC and TA in the Strait of Georgia is surface-intensified (Moore-Maley et al., 2016), we use surface (3 m average) DIC:TA ratio, pH and Ω_A as our primary model sensitivity metrics.

3 Results

3.1 Sensitivity to physical forcing

Freshwater forcing exerts strong control over model biology (nutrients, light, phytoplankton, zooplankton) and carbonate chemistry (DIC, TA, pH, Ω_A), particularly during summer (Moore-Maley et al., 2016). Although the model is forced by a combination of the Fraser River and local rainfall-dominated rivers, the Fraser accounts for most of the summer freshwater signal. The Fraser River flow record at Hope during the 12 year period from 2001 through 2012 is seasonally and interannually variable in terms of freshet size, timing, and duration with the smallest freshet (in 2010) just under 6000 m^3 s^{-1} and the largest freshet (in 2012) just under 12000 m^3 s^{-1} (Fig 3a). Model salinity (3 m averaged) is strongly inversely related to this freshwater signal and reaches a minimum of approximately 15 in 2010 and 5 in 2012 (Fig 3b). Winter rainfall pulses and their effect on winter salinity are evident particularly in February 2005. However several winter salinity dips appear without noticeable corresponding pulses in the Fraser Record. These events are likely forced by the scaled Englishman River record (not shown). Overall, aside from a handful of stronger winter salinity dips, a salinity threshold of ~20 appears to separate the summer high flow period from the lower background flow regime.

Model DIC:TA, pH and Ω_A (3 m averaged) during 2010 and 2012 all demonstrate strong seasonal variability between winter and summer (Fig. 4) which can be attributed to the seasonal cycle of productivity that is characteristic of the region and persistent in the model (Moore-Maley et al., 2016). Prior to the summer, differences between the two years arise primarily due to variable wind and irradiance affecting the onset and termination of spring blooms. During summer, interannual variability

5 of Fraser River discharge drives larger changes between the two years. In 2010, throughout the summer, biological drawdown of DIC remains strong keeping DIC:TA low and pH and Ω_A high (red lines, Fig. 4). However, in summer 2012 DIC drawdown weakens due to river shading caused by river turbidity, thus increasing DIC and DIC:TA and significantly lowering pH and Ω_A (black lines, Fig. 4). Meanwhile, superimposed on top of this physical-biological response, the effects of river chemistry begin to emerge. During the summer, model DIC:TA and pH vary across the 6 TA_f cases (Fig. 4a and b, gray/pink lines) by

10 approximately half of the total difference between years (black − red) at peak freshet. This variability across TA_f cases is not evident for model Ω_A.

To investigate the impact of flow dependent TA_f we consider the Medium Carbon, flow dependent TA_f case. The strongest TA_f variations ($\sim$100–400 μmol kg^{-1}) occur during the summer (Fig. 5a) due to the rapid rising and falling discharge rates associated with the Fraser River freshet (Fig 3a). Positive TA_f deviations during rising water at the beginning of the freshet

15 cause an overall decrease in pH and Ω_A (3 m averaged), although the timing of these events can vary depending on the freshet timing. For example, model pH and Ω_A decrease by 0.1 and 0.07, respectively, in June 2007 and May 2008 (Fig. 5b and c) due to the large TA_f increase (Fig 5a), and associated DIC_f increase, during the rapid early progression to freshet in those years (Fig 3a). In contrast, the freshet in 2012, although larger, progresses more slowly (Fig 3a) and the model pH and Ω_A decreases are thus smaller and occur at different times in the season (Fig. 5b and c). Following the freshet, negative TA_f deviations

20 during falling water cause an overall increase in pH and Ω_A, although the increase is not as strong as the pre-freshet decrease for pH (Fig. 5b). While these changes are significant (e.g., ΔpH = 0.1 and Ω_A = 0.07 at times), they are small relative to the differences across the range of TA_f scenarios (Fig. 4) and practically insignificant relative to the differences between low and high flow years (e.g., 2010 and 2012, Fig. 4). Furthermore, the model pH and Ω_A deviations caused by flow-dependent TA_f are moderately symmetric about the freshet, so that time-averaged results will likely be similar to the results of a constant

25 TA_f scenario. Thus flow dependence is likely less important than other factors when considering freshwater chemistry in this system, however, it could play an important role on daily to weekly timescales.

3.2 Sensitivity to river chemistry

In order to examine the response of the model across the range of TA_f for all years and across all three freshwater carbon (DIC_f:TA_f) scenarios, similar to our analysis of 2010 versus 2012 at Med Carbon (DIC_f:TA_f = 1.089, Fig. 4), it is useful to

30 look at the model results as time averages. We identified a model salinity of 20 to be an approximate threshold separating the summer flow regime from the background flow during the rest of the year. We thus time average our results over the period where salinity < 20 using the same three metrics (3 m averaged DIC:TA, pH, Ω_A) as in Fig. 4 and the same flow year color scheme as in Fig. 3 to produce a comprehensive summary of our 216 model runs (18 freshwater chemistry scenarios $\times$ 12 years of freshwater, wind and meteorological forcing) at low salinity (Fig. 6). The sensitivity of the model to differences in

river discharge between years (e.g., red and black lines, Fig. 4) is clear in these low salinity time averages as the spread of points along the vertical axis at a given TA_f, with 2010 and 2012 again highlighted (red and black stars, Fig. 6). The sensitivity of the model to TA_f (e.g., pink and gray lines, Fig. 4) is also clear as the trend along the horizontal axis for a given year in each panel (Fig. 6).

Time averaged (salinity < 20) model DIC:TA increases with increasing TA_f in all three river carbon cases (Fig. 6a-c) causing a decreasing trend in model pH (Fig. 6d-f). These trends are weak in the Low Carbon scenario such that the response to TA_f is weaker than the response to freshwater flow (Figs. 6a and d). Conversely in the High Carbon scenario, the increase in model DIC:TA and decrease in model pH with TA_f are significantly stronger than the corresponding responses to freshwater flow (Figs. 6c and f). These results show that a high carbon freshwater endmember produces a stronger estuarine carbon chemistry response than a low carbon freshwater endmember.

The response of model Ω_A to freshwater chemistry is more complicated. First of all, the dominance of freshwater flow over freshwater chemistry in determining model Ω_A between 2010 and 2012 (Fig 4c) is robust throughout the 18 freshwater chemistry scenarios as evident by the large vertical spread at a given TA_f relative to the trends along the horizontal axis (Figs. 6g-i). Secondly, model Ω_A increases with TA_f in the Low Carbon scenario despite increasing model DIC:TA and decreasing model pH (Figs. 6a, d and g) because increasing DIC also increases the carbonate ion concentration in this case. Then in the High Carbon scenario, model Ω_A reverses its sensitivity to TA_f to follow the model pH trend (Figs. 6f and i). In this case the shift within the DIC pool toward dissolved CO_2 causes a sufficient reduction in the carbonate ion, so that increasing DIC no longer increases $[CO_3^{2-}]$.

4 Discussion

4.1 Mechanisms influencing sensitivity

To conceptualize the results, especially the non-intuitive (such as low pH at high TA_f), we calculate conservative mixing curves between model freshwater and seawater endmembers (Table 1) for 6 different river chemistry scenarios; specifically, at low TA_f (solid lines) and high TA_f (dashed lines) across the Low (magenta), Med (black) and High (yellow) Carbon scenarios (Fig. 7a-c). We compared model results (daily averages in salinity space) for the largest freshet year (2012) with these curves. There are strong similarities below S $\sim$ 15 in the way that estuarine DIC:TA, pH, and Ω_A are affected by river chemistry. For example, increasing Carbon shifts both theoretical curves and model points in the same direction and by about the same amount; e.g., (Fig. 7a-c). The pH shift between high and low TA_f curves at High Carbon is about 0.2 for both theory and model (Fig 7b). These variations with freshwater chemistry changes are analogous to the trends discussed in Sect. 3.2 (Fig. 6).

The mixing curves illustrate that increasing TA_f within a given DIC_f:TA_f scenario results in a greater contribution of DIC to the estuary relative to TA. This carbon increase is seen most clearly in the difference of the DIC and TA mixing curves, DIC$-$TA (Fig 7d), but is also evident by comparing the DIC:TA curves between the low and high TA_f cases (Fig 7a). For DIC:TA, the endmember ratios are the same in both TA_f cases, but the ratio within the estuary is different. The extra DIC

in the estuary is what causes pH and Ω_A to decrease with increasing TA_f. These decreases are strongest in the High Carbon scenario (e.g., Fig. 6f and i) because DIC_f:TA_f is larger, and thus the excess DIC contribution to the estuary is higher between TA_f scenarios (yellow curves, Fig 7d).

Model Ω_A responds differently to TA_f under each of the three freshwater carbon scenarios, reversing its trend between Low Carbon and High Carbon. The mixing curves demonstrate a similar pattern (Fig. 7c) where the Med Carbon scenario appears to define a threshold at which Ω_A diverges from its similarity to pH in response to TA_f. The responses of model pH and Ω_A to freshwater carbonate chemistry changes in this system are thus asynchronous. We attribute this asynchrony to higher estuarine carbonate in the high TA_f case which is able to buffer effectively against the equilibrium-driven carbonate loss that accompanies rising estuarine DIC:TA, but only in the Med and High Carbon scenarios. In the Low Carbon scenario, the equilibrium-driven carbonate loss is too strong.

While the trends of the model with changing freshwater scenarios are similar to those of the endmember mixing curves, the striking differences highlight the importance of biology and gas exchange in reducing unfavorable carbonate chemistry conditions in the Fraser River – Strait of Georgia system. The model converges tightly to the seawater endmember for most of the winter, but estuarine carbon decreases significantly during the spring phytoplankton bloom (green arrows, Fig. 7a). The model remains carbon deficient relative to the mixing curves throughout the year, only partially converging toward the freshwater endmember during the freshet. The model then retraces its carbon deficient path toward higher salinity and only converges back to the seawater endmember after fall phytoplankton blooms terminate (blue arrows, Fig. 7a). Most importantly, while biology and gas exchange do not completely buffer the effects of freshwater chemistry in the model, they do shift the system toward a significantly lower carbon state than would be found under mixing alone.

4.2 Comparison to other rivers and implications for future climate

Present-day carbonate chemistry in world rivers covers a large range (DIC or TA from $\sim$50 to 7000 μmol kg^{-1}; Fig. 8). Pollution drives part of this variability (black symbols, Fig. 8) as does latitude, in large part from the presence of carbonate rocks in many temperate drainage basins (Amiotte Suchet et al., 2003) – the tropical Amazon and Congo rivers have exceedingly low TA and DIC by contrast (cyan symbols, Fig. 8). In some rivers seasonal variability of DIC and TA far exceeds that of the Fraser. This variability is particularly high in the polluted rivers and also the Yukon. However overall, the range of DIC:TA in most rivers is near or within the range determined for this study. The tropical rivers are an exception. The Congo River (cyan square, Fig. 8c and d), for example, has nearly constant DIC throughout the year while TA drops to less than half of the DIC concentration at peak river discharge (Wang et al., 2013). Another exception is cold glacial melt water (magenta square), which even at a DIC:TA more than twice as high as our High Carbon scenario, is pCO$_2$-undersaturated relative to the atmosphere and continues to take up DIC as it mixes with seawater (Meire et al., 2015). Seasonal biological productivity may also regulate DIC in some temperate rivers, at least near the river mouth, as it does in the Fraser River. In the Columbia River estuary, DIC drawdown is strong in the spring, but is replaced by net heterotrophy during the summer and fall. This early transition to heterotrophy makes the Columbia estuary a net annual source of CO$_2$ to the atmosphere (Evans et al., 2013) despite maintaining a relatively low DIC:TA ratio (yellow square, Fig. 8). The Fraser estuary by contrast has a significantly

higher DIC:TA ratio, but maintains a seasonally-persistent $p\mathrm{CO_2}$-undersaturation relative to the atmosphere because of strong productivity throughout most summers.

In the coming decades, weathering rates and mean river TA are unlikely to change significantly due to climate (Riebe et al., 2001). In contrast, increasing atmospheric $p\mathrm{CO_2}$ will increase DIC in the ocean and most likely in rivers as well. River DIC may be influenced by many additional variables, including changes in freshwater flow, human pressures (local anthropogenic inputs) and anticipated increases in river temperature. For example, the relatively high DIC:TA ratio of the present day glacial DIC and TA end-member (magenta square, Fig. 8c, d) is in equilibrium with the atmosphere at a river temperature of $0^{\circ}\mathrm{C}$ (Meire et al., 2015), but if this pure glacier water were to experience a $10^{\circ}\mathrm{C}$ increase during its passage to the ocean, then outgassing would decrease river DIC by about 10% ($\sim 9~\mu\mathrm{mol~kg^{-1}}$) if the melt water remained in atmospheric equilibrium. However, its pH would stay about the same (slight increase) in this scenario. More generally, ocean pH will become more sensitive to changes in dissolved $\mathrm{CO_2}$ as the oceans become warmer and higher in overall $\mathrm{CO_2}$ because of weakening buffer capacity (Hagens and Middelburg, 2016). Were this trend to be significant in the Strait of Georgia, it would further exacerbate the increased estuarine pH and Ω_A sensitivity that we observe at high river DIC in the biogeochemical model.

In addition to freshwater chemistry, the large seasonal freshwater flux from the Fraser River exerts a significant influence on estuarine pH, and particularly Ω_A, in the Strait of Georgia, with the highest flow years producing the most acidic and corrosive conditions. The Strait is relatively acidic throughout the water column compared to its primary conduit to the Pacific Ocean, the Juan de Fuca Strait, as well as the British Columbia continental shelf during upwelling (Ianson et al., 2016). The surface Strait of Georgia is also relatively acidic compared with oceanic extrapolations of fresh water endmembers from the otherwise similar, glacially-fed temperate Corcovado estuary in Chile (Torres et al., 2011), despite the higher extrapolated TA in the Fraser relative to the Corcovado estuary's primary freshwater source, the Puelo River. This excess background DIC may contribute significantly to the persistent surface aragonite undersaturation observed (Ianson et al., 2016) and modeled (Moore-Maley et al., 2016) in the Strait during winter and during large summer freshets.

A warming climate has (Zhang et al., 2001) and will continue (Morrison et al., 2014) to reduce the peak freshet flows of glacial, temperate rivers and move the freshet timing earlier, which may reduce the severity of summer aragonite undersatura-tion in the Strait of Georgia associated with large freshets. Winter flows may also increase, however, which could increase the sensitivity of the estuary to river chemistry during these low flow times beyond our model (currently insensitive) predictions. A changing freshet climatology may affect the significance of freshwater TA flow dependence as well. While many different studies consider flow dependent river TA to anticorrelate with discharge (e.g., Wang et al., 2013; Evans et al., 2013), the strong Fraser River TA hysteresis demonstrated by our data links the strongest Fraser River TA fluctuations to rapid pulses in river discharge. A future shift to smaller freshets will thus likely reduce the already weak influence of flow dependent freshwater TA in the model, supporting the use of fixed freshwater TA endmembers in large scale acidification projection models (e.g., Volta et al., 2016). However, the present study highlights the importance of choosing a freshwater TA endmember carefully.

5   Conclusions

The Fraser River is a large, free-flowing, glacially fed river that exerts a strong physical and chemical influence on a neighboring, semi-enclosed estuarine sea, the Strait of Georgia, that is DIC-rich relative to the open ocean. Based on recent data, we find that the Fraser River is moderately alkaline (TA = 500–1000 μmol kg^{-1}) but appears to carry a significant DIC load (high DIC:TA) even relative to many world rivers. TA appears to vary systematically with river flow, but does not display a simple dilution relationship. Rather it exhibits a strong hysteresis such that TA is a function of the change with respect to time in river flow.

We examined the sensitivity of Ω_A and pH in the Strait of Georgia to Fraser River carbonate chemistry by summarizing the results of a coupled biogeochemical model across 12 hydrological cycles and 18 freshwater TA and DIC:TA combinations. Model results show that estuarine pH and Ω_A are strongly sensitive to river flow and river carbonate chemistry at moderate to low model salinities (< 20), and generally decrease as river flow or river DIC increases. The primary reason for this sensitivity is the strong estuarine DIC regulation achieved both by physical river shading effects on primary productivity, and by the DIC contribution relative to TA from the freshwater endmember to the estuary.

Model DIC and pH are tightly coupled by the dominant influence of the carbonate equilibrium, however estuarine Ω_A responds asynchronously from DIC and pH to increasing freshwater TA at low and moderate freshwater DIC:TA (which we consider to represent past and present) scenarios as river DIC:TA approaches unity. Under these conditions the carbonate ion follows DIC and simple dilution/enhancement controls Ω_A. This estuarine Ω_A response reverses when freshwater DIC:TA becomes larger ($>\sim1.1$) because the carbonate ion makes up an increasingly smaller portion of the total DIC and the Ω_A dynamics are thus no longer controlled by physical dilution. In our highest freshwater DIC:TA scenario, Ω_A responds to estuarine DIC:TA similarly to pH.

The Fraser river estuary is biological productive, which modulates its sensitivity to river chemistry. In winter, productivity is low so estuary chemistry nearly follows simple endmember mixing theory. Once the seasonal phytoplankton bloom occurs and there is significant biological drawdown of DIC, both estuarine pH and Ω_A increase away from the physical mixing line. Thus, even though the river flow is at a maximum during summer, estuarine sensitivity to river chemistry (in particular to DIC) is significantly reduced. Finally, the strong impact of Fraser River flow input on pH and Ω_A in the Strait of Georgia will be reduced as the Fraser watershed makes its expected transition to smaller, earlier freshets with climate change. However, if DIC:TA ratios increase in one or both of the river-ocean endmembers as anticipated with rising atmospheric CO_2, then the increased sensitivity of estuarine pH and Ω_A associated with this endmember change may counteract the flow regime changes to some degree.

Code and data availability.   Model source code and run scripts are available from the UBC Salish Sea bitbucket repository https://bitbucket.org/account/user/salishsea/projects/SOG. Results files for the sensitivity experiments will be hosted at the Abacus Dataverse Network which is a research data repository of the British Columbia Research Libraries' Data Services http://dvn.library.ubc.ca/dvn, prior to publication. Model initialization data is available from the Fisheries and Oceans Canada Institute of Ocean Sciences Data Archive http://www.pac.

dfo-mpo.gc.ca/science/oceans/data-donnees/search-recherche/profiles-eng.asp. Carbon cruise data from the Fraser River plume presented in Ianson et al. (2016) and additional new observations from two field campaigns will be hosted at the U.S. Department of Energy's ESS-DIVE data repository prior to publication. All other data presented in this article are available from their cited URL locations.

Competing interests. The authors declare that they have no conflict of interest.

5 *Acknowledgements.* This work was supported by a Natural Sciences and Engineering Research Council of Canada (NSERC) Discovery grant to the third author, Fisheries and Oceans Canada's Climate Change Science Initiative and International Governance Strategy programs, and the Marine Environmental Observation, Prediction, and Response (MEOPAR) Network of Centres of Excellence of Canada. We thank Diane Masson and Peter Chandler (IOS) for sharing their Strait of Georgia survey data, and Eleanor Simpson and Karen Kohfeld (Simon Fraser University), Marty Davelaar (IOS), Yves Perrault (Little Wing Oysters) and Andre Comeau (Okeover Organic Oysters) for collecting 10 and sharing data from the Freke Ancho River. We thank Doug Latornell at UBC for developing the model working environment, and Robie Macdonald and Paul Covert for providing helpful insights. The second author thanks Niki Gruber for his hospitality at ETH-Zurich while this manuscript was completed. We also acknowledge five anonymous reviewers for their detailed feedback.

References

Allen, S. E. and Wolfe, M. A.: Hindcast of the timing of the spring phytoplankton bloom in the Strait of Georgia, 1968-2010, Prog. Oceanogr., 115, 6–13, doi:10.1016/j.pocean.2013.05.026, 2013.

Allen, S. E., Latornell, D., Olson, E., and Pawlowicz, R.: Timing of the spring phytoplankton bloom in the Strait of Georgia, 2015 and 2016., in: State of the physical, biological and selected fishery resources of Pacific Canadian marine ecosystems in 2015., edited by Chandler, P., King, S., and Perry, I., vol. 3179, pp. 147–152, Can. Tech. Rep. Fish. Aquat. Sci., Canada, 2016.

Amiotte Suchet, P., Probst, J., and Ludwig, W.: Worldwide distribution of continental rock lithology: Implications for the atmospheric/soil CO_2 uptake by continental weathering and alkalinity river transport to the oceans, Glob. Biogeochem. Cycles, 17, 1038, doi:10.1029/2002GB001891, 2003.

Bianucci, L., Denman, K. L., and Ianson, D.: Low oxygen and high inorganic carbon on the Vancouver Island Shelf, J. Geophys. Res. Oceans, 116, C07011, doi:10.1029/2010JC006720, 2011.

Cai, W.: Riverine inorganic carbon flux and rate of biological uptake in the Mississippi River plume, Geophys. Res. Lett., 30, 1032, doi:10.1029/2002GL016312, 2003.

Cai, W., Wang, Y., and Hodson, R. E.: Acid-base properties of dissolved organic matter in the estuarine waters of Georgia, USA, Geochim. Cosmochim. Ac., 62, 473–483, doi:10.1016/S0016-7037(97)00363-3, 1998.

Cai, W., Guo, X., Chen, C. A., Dai, M., Zhang, L., Zhai, W., Lohrenz, S. E., Yin, K., Harrison, P. J., and Wang, Y.: A comparative overview of weathering intensity and HCO_3^- flux in the world's major rivers with emphasis on the Changjiang, Huanghe, Zhujiang (Pearl) and Mississippi Rivers, Cont. Shelf. Res., 28, 1538–1549, doi:10.1016/j.csr.2007.10.014, 2008.

Cai, W., Hu, X., Huang, W., Murrell, M. C., Lehrter, J. C., Lohrenz, S. E., Chou, W., Zhai, W., Hollibaugh, J. T., Wang, Y., Zhao, P., Guo, X., Gundersen, K., Dai, M., and Gong, G.: Acidification of subsurface coastal waters enhanced by eutrophication, Nature Geosci., 4, 766–770, doi:10.1038/ngeo1297, 2011.

Cai, W.-J., Huang, W.-J., Luther, G. W., Pierrot, D., Li, M., Testa, J., Xue, M., Joesoef, A., Mann, R., Brodeur, J., Xu, Y.-Y., Chen, B., Hussain, N., Waldbusser, G. G., Cornwell, J., and Kemp, W. M.: Redox reactions and weak buffering capacity lead to acidification in the Chesapeake Bay, Nature Communications, 8, doi:doi:10.1038/s41467-017-00417-7, 2017.

Cameron, E. M. and Hattori, K.: Strontium and neodymium isotope ratios in the Fraser River, British Columbia: a riverine transect across the Cordilleran orogen, Chem. Geol., 137, 243–253, doi:10.1016/S0009-2541(96)00168-4, 1997.

Cloern, J. E., Foster, S. Q., and Kleckner, A. E.: Phytoplankton primary production in the world's estuarine-coastal ecosystems, Biogeosci., 11, 2477–2501, doi:10.5194/bg-11-2477-2014, 2014.

Cloern, J. E., Abreu, P. C., Carstensen, J., Chauvaud, L., Elmgren, R., Grall, J., Greening, H., Johansson, J. O. R., Kahru, M., Sherwood, E. T., Xu, J., and Yin, K.: Human activities and climate variability drive fast-paced change across the world's estuarine-coastal ecosystems, Glob. Change Biol., 22, 513–529, doi:10.1111/gcb.13059, 2015.

Collins, A. K., Allen, S. E., and Pawlowicz, R.: The role of wind in determining the timing of the spring bloom in the Strait of Georgia, Can. J. Fish. Aquat. Sci., 66, 1597–1616, doi:10.1139/F09-071, 2009.

Covington, A. K., Whalley, P. D., and Davison, W.: Procedures for the measurement of pH in low ionic strength solutions including freshwater, Analyst, 108, 1528–1532, doi:10.1039/AN9830801528, 1983.

de Fátima F. L. Rasera, M., Krusche, A. V., E.Richey, J., Ballester, M. V. R., and Victória, R. L.: Spatial and temporal variability of pCO_2 and CO_2 efflux in seven Amazonian rivers, Biogeochemistry, 116, 241–259, doi:10.1007/s10533-013-9854-0, 2013.

Dickson, A. G., Sabine, C. L., and Christian, J. R.: Guide to Best Practices for Ocean CO_2 Measurements, PICES Special Publication 3, cdiac.ornl.gov/oceans/Handbook_2007.html, 2007.

Ethier, A. and Bedard, J.: Development of a real-time water quality buoy for the Fraser River Estuary, AXYS Technologies Inc., Sidney, British Columbia, 2007.

5   Evans, W., Hales, B., and Strutton, P. G.: pCO_2 distributions and air-water CO_2 fluxes in the Columbia River estuary, Estuar. Coast. Shelf Sci., 117, 260–272, doi:10.1016/j.ecss.2012.12.003, 2013.

Fennel, K., Hu, J., Laurent, A., Marta-Almeida, M., and Hetland, R.: Sensitivity of hypoxia predictions for the northern Gulf of Mexico to sediment oxygen consumption and model nesting, J. Geophys. Res. Oceans, 118, 990–1002, doi:10.1002/jgrc.20077, 2013.

Frankignoulle, M., Bourge, I., and Wollast, R.: Atmospheric CO_2 fluxes in a highly polluted estuary (the Scheldt), Limnol. Oceanogr., 41, 365–369, doi:10.4319/lo.1996.41.2.0365, 1996.

Hagens, M. and Middelburg, J. J.: Generalised expressions for the response of pH to changes in ocean chemistry, Geochimica et Cosmochimica Acta, 187, 334 – 349, doi:https://doi.org/10.1016/j.gca.2016.04.012, 2016.

Haigh, R., Ianson, D., Holt, C. A., Neate, H. E., and Edwards, A. M.: Effects of ocean acidification on temperate coastal marine ecosystems and fisheries in the Northeast Pacific, PLoS ONE, 10, e0117533, doi:doi:10.1371/journal.pone.0117533, 2015.

15   Harrison, P. J., Fulton, J. D., Taylor, F. J. R., and Parsons, T. R.: Review of the biological oceanography of the Strait of Georgia: pelagic environment, Can. J. Fish. Aquat. Sci., 40, 1064–1094, doi:10.1139/f83-129, 1983.

Hellings, L., Dehairs, F., Damme, S. V., and Baeyens, W.: Dissolved inorganic carbon in a highly polluted estuary (the Scheldt), Limnol. Oceanogr., 46, 1406–1414, doi:10.4319/lo.2001.46.6.1406, 2001.

Hernández-Ayón, J. M., Zirino, A., Dickson, A. G., Camiro-Vargas, T., and Valenzuela-Espinoza, E.: Estimating the contribu-

20   tion of organic bases from microalgae to the titration alkalinity in coastal seawaters, Limnol. Oceanogr. Methods, 5, 225–232, doi:10.4319/lom.2007.5.225, 2007.

Hofmann, A. F., Middleburg, J. J., Soetaert, K., and Meysman, F. J. R.: pH modelling in aquatic systems with time-variable acid-base dissociation constants applied to the turbid, tidal Scheldt estuary, Biogeosci., 6, 1539–1561, doi:10.5194/bg-6-1539-2009, 2009.

Hu, X. and Cai, W.: Estuarine acidification and minimum buffer zone — A conceptual study, Geophys. Res. Lett., 40, 5176–5181,

25   doi:10.1002/grl.51000, 2013.

Hunt, C. W., Salisbury, J. E., and Vandemark, D.: Contribution of non-carbonate anions to total alkalinity and overestimation of pCO_2 in New England and New Brunswick rivers, Biogeosci., 8, 3069–3076, doi:10.5194/bg-8-3069-2011, 2011.

Hunt, C. W., Salisbury, J. E., and Vandemark, D.: CO_2 input dynamics and air-sea exchange in a large New England estuary, Estuar. Coast., 37, 1078–1091, doi:10.1007/s12237-013-9749-2, 2014.

30   Ianson, D., Allen, S. E., Moore-Maley, B. L., Johannessen, S. C., and Macdonald, R. W.: Vulnerability of a semi-enclosed estuarine sea to ocean acidification in contrast with hypoxia, Geophys. Res. Lett., 43, 5793–5801, doi:10.1002/2016GL068996, 2016.

Jiang, L., Feely, R. A., Carter, B. R., Greeley, D. J., Gledhill, D. K., and Arzayus, K. M.: Climatological distribution of aragonite saturation state in the global oceans, Glob. Biogeochem. Cycles, 29, 1656–1673, doi:10.1002/2015GB005198, 2015.

Kennedy, V. C.: Minerology and cation-exchange capacity of sediments from selected streams, Prof. Paper 433-D, U.S. Geol. Surv., 1965.

35   Kim, H. and Lee, K.: Significant contribution of dissolved organic matter to seawater alkalinity, Geophys. Res. Lett., 36, L20603, doi:10.1029/2009GL040271, 2009.

Koeve, W. and Oschlies, A.: Potential impact of DOM accumulation on fCO_2 and carbonate ion computations in ocean acidification experiments, Biogeosci., 9, 3787–3798, doi:10.5194/bg-9-3787-2012, 2012.

Large, W. G., McWilliams, J. C., and Doney, S. C.: Oceanic vertical mixing: a review and a model with a nonlocal boundary layer parametrization, Rev. Geophys., 32, 363–403, doi:10.1029/94RG01872, 1994.

LeBlond, P. H.: The Strait of Georgia: functional anatomy of a coastal sea, Can. J. Fish. Aquat. Sci., 40, 1033–1063, doi:10.1139/f83-128, 1983.

5   Lewis, E. R. and Wallace, D. W. R.: Program Developed for CO_2 System Calculations, DOE (U.S. Department of Energy), ORNL/CDIAC-105, 1998.

Masson, D.: Seasonal water mass analysis for the Straits of Juan de Fuca and Georgia, Atmos. Ocean, 44, 1–15, doi:10.3137/ao.440101, 2006.

Masson, D. and Peña, A.: Chlorophyll distribution in a temperate estuary: The Strait of Georgia and Juan de Fuca Strait, Estuarine Coastal

10   Shelf Sci., 82, 19–28, doi:10.1016/j.ecss.2008.12.022, 2009.

Meire, L., Søgaard, D. H., Mortensen, J., Meysman, R. J. R., Soetaert, K., Arendt, K. E., Juul-Pedersen, T., Blicher, M. E., and Rysgaard, S.: Glacial meltwater and primary production are drivers of strong CO2 uptake in fjord and coastal waters adjacent to the Greenland Ice Sheet, Biogeosciences, 12, 2347–2363, 2015.

Meybeck, M.: Global chemical weathering of surficial rocks estimated from river dissolved loads, Am. J. Sci., 287, 401–428,

15   doi:10.2475/ajs.287.5.401, 1987.

Millero, F. J.: Carbonate constants for estuarine waters, Mar. Fresh. Res., 61, 139–142, doi:10.1071/MF09254, 2010.

Moore-Maley, B. L., Allen, S. E., and Ianson, D.: Locally-driven interannual variability of near-surface pH and Ω_A in the Strait of Georgia, J. Geophys. Res. Oceans, 121, 1600–1625, doi:10.1002/2015JC011118, 2016.

Morrison, J., Callendar, W., Foreman, M. G. G., Masson, D., and Fine, I.: A model simulation of future oceanic conditions along the British

20   Columbia continental shelf. Part I: Forcing fields and initial conditions, Atmos. Ocean, 52, 1–19, doi:10.1080/07055900.2013.868340, 2014.

Nightingale, P. D., Malin, G., Law, C. S., Watson, A. J., Liss, P. S., Liddicoat, M. I., Boutin, J., and Upstill-Goddard, R. C.: In situ evaluation of air-sea gas exchange parametrizations using novel conservative and volatile tracers, Global Biogeochem. Cycles, 14, 373–387, doi:10.1029/1999GB900091, 2000.

25   Pawlowicz, R., Riche, O., and Halverson, M.: The circulation and residence time of the Strait of Georgia using a simple mixing-box approach, Atmos. Ocean, 45, 173–193, doi:10.3137/ao.450401, 2007.

Peña, A., Masson, D., and Callendar, W.: Annual plankton dynamics in a coupled physical-biological model of the Strait of Georgia, British Columbia, Prog. Oceanogr., 146, 58–74, doi:10.1016/j.pocean.2016.06.002, 2016.

Preston-Thomas, H.: The international temperature scale of 1990 (ITS-90), Metrologia, 27, 3–10, doi:10.1088/0026-1394/27/1/002, 1990.

30   Riche, O.: Time-dependent inverse box-model for the estuarine circulation and primary productivity in the Strait of Georgia, Ph.D. thesis, University of British Columbia, 2011.

Richey, J. E., Hedges, J. I., Devol, A. H., Quay, P. D., Victoria, R., Martinelli, L., and Forsberg, B. R.: Biogeochemistry of carbon in the Amazon River, Limnol. Oceanogr., 35, 352–371, doi:10.4319/lo.1990.35.2.0352, 1990.

Riebe, C. S., Kirchner, J. W., Granger, D. E., and Finkel, R. C.: Strong tectonic and weak climatic control of long-term chemical weathering

35   rates, Geol., 29, 511–514, doi:10.1130/0091-7613(2001)029<0511:STAWCC>2.0.CO;2, 2001.

Riley, J. P. and Tongudai, M.: The major cation/chlorinity ratios in sea water, Chem. Geol., 2, 263–269, doi:10.1016/0009-2541(67)90026-5, 1967.

Roegner, G. C., Seaton, C., and Baptista, A. M.: Climatic and tidal forcing of hydrography and chlorophyll concentrations in the Columbia River Estuary, Estuar. Coast., 34, 281–296, doi:10.1007/s12237-010-9340-z, 2011.

Salisbury, J., Green, M., Hunt, C., and Campbell, J.: Coastal acidification by rivers: a threat to shellfish?, Eos Trans. AGU, 89, 513, doi:10.1029/2008EO500001, 2008.

5   Sarmiento, J. L. and Gruber, N.: Ocean Biogeochemical Dynamics, Princeton University Press, 2006.

Schindler, D. W.: Effects of acid rain on freshwater ecosystems, Science, 239, 149–157, doi:10.1126/science.239.4836.149, 1988.

Torres, R., Pantoja, S., Harada, N., González, H. E., Daneri, G., Frangopulos, M., Rutllant, J. A., Duarte, C. M., Rúiz-Halpern, S., Mayol, E., and Fukasawa, M.: Air-sea CO2 fluxes along the coast of Chile: From CO2 outgassing in central northern upwelling waters to CO2 uptake in southern Patagonian fjords, Journal of Geophysical Research: Oceans, 116, doi:10.1029/2010JC006344, http://dx.doi.org/10.

10   1029/2010JC006344, c09006, 2011.

UNESCO: The Practical Salinity Scale 1978 and the International Equation of State of Seawater 1980, Tech. rep., UNESCO technical papers in marine science No. 36, 1981.

Volta, C., Laruelle, G. G., Arndt, S., and Regnier, P.: Linking biogeochemistry to hydro-geometrical variability in tidal estuaries: a generic modeling approach, Hydrol. Earth Syst. Sci., 20, 991–1030, doi:10.5194/hess-20-991-2016, 2016.

15   Voss, B. M., Peucker-Ehrenbrink, B., Eglinton, T. I., Fiske, G., Wang, Z. A., Hoering, K. A., Montluçon, D. B., LeCroy, C., Pal, S., Marsh, S., Gillies, S. L., Janmaat, A., Bennett, M., Downey, B., Fanslau, J., Fraser, H., Macklam-Harron, G., Martinec, M., and Wiebe, B.: Tracing river chemistry in space and time: dissolved inorganic constituents of the Fraser River, Canada, Geochim. Cosmochim. Ac., 124, 283–308, doi:10.1016/j.gca.2013.09.006, 2014.

Waldbusser, G. G. and Salisbury, J. E.: Ocean acidification in the coastal zone from an organism's perspective: multiple system parameters,

20   frequency domains, and habitats, Ann. Rev. Mar. Sci., 6, 221–247, doi:10.1146/annurev-marine-121211-172238, 2014.

Waldbusser, G. G., Hales, B., Langdon, C. J., Haley, B. A., Schrader, P., Brunner, E. L., Gray, M. W., Miller, C. A., and Gimenez, I.: Saturation-state sensitivity of marine bivalve larvae to ocean acidification, Nat. Clim. Change, 5, 273–280, doi:10.1038/nclimate2479, 2015.

Wang, Z. A., Bienvenu, D. J., Mann, P. J., Hoering, K. A., Poulsen, J. R., Spencer, R. G. M., and Holmes, R. M.: Inorganic carbon speciation

25   and fluxes in the Congo River, Geophys. Res. Lett., 40, 511–516, doi:10.1002/grl.50160, 2013.

Wanninkhof, R.: Relationship between wind speed and gas exchange over the ocean, J. Geophys. Res., 97, 7373–7382, doi:10.1029/92JC00188, 1992.

Weiss, R. F.: Carbon dioxide in water and seawater: the solubility of a non-ideal gas, Mar. Chem., 2, 203–215, doi:10.1016/0304-4203(74)90015-2, 1974.

30   Wheeler, J. O., Brookfield, A. J., Gabrielse, H., Monger, J. W. H., Tipper, H. W., and Woodsworth, G. J.: Terrane map of the Canadian Cordillera, Map 1713A, Geol. Surv. Can., scale 1:200,000, 1991.

Xue, L., Cai, W.-J., Sutton, A. J., and Sabine, C.: Sea surface aragonite saturation state variations and control mechanisms at the Gray's Reef time-series site off Georgia, USA (2006-2007), Marine Chemistry, 195, 27 – 40, doi:https://doi.org/10.1016/j.marchem.2017.05.009, 2017.

35   Zhai, W., Dai, M., and Guo, X.: Carbonate system and CO_2 degassing fluxes in the inner estuary of Changjiang (Yangtze) River, China, Mar. Chem., 107, 342–356, doi:http://dx.doi.org/10.1016/j.marchem.2007.02.011, 2007.

Zhang, X., Havery, K. D., Hogg, W. D., and Yuzyk, T. R.: Trends in Canadian Streamflow, Water Resources Res., 37, 987–998, doi:10.1029/2000WR900357, 2001.
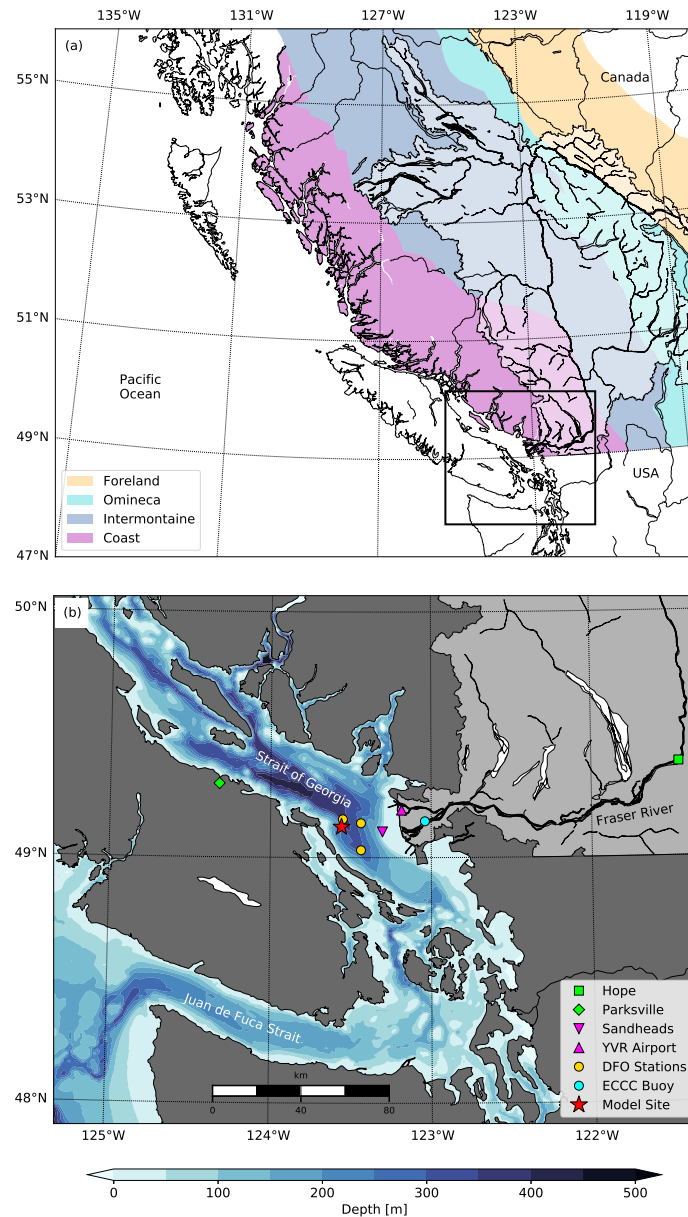
Figure 1. Maps of (a) the Fraser River watershed showing the major geologic belts (Wheeler et al., 1991), and (b) the lower Fraser River and Strait of Georgia showing the model location (red star), Environment and Climate Change Canada (ECCC) meteorological (Sandheads and YVR, magenta symbols) and river gauging (Fraser River at Hope and Englishman River at Parksville, green symbols) stations used to force the model, and Fisheries and Oceans Canada (DFO) sampling stations (yellow circles) and the ECCC Fraser River Water Quality Buoy (cyan circle) used to constrain Fraser River TA and pH, respectively.
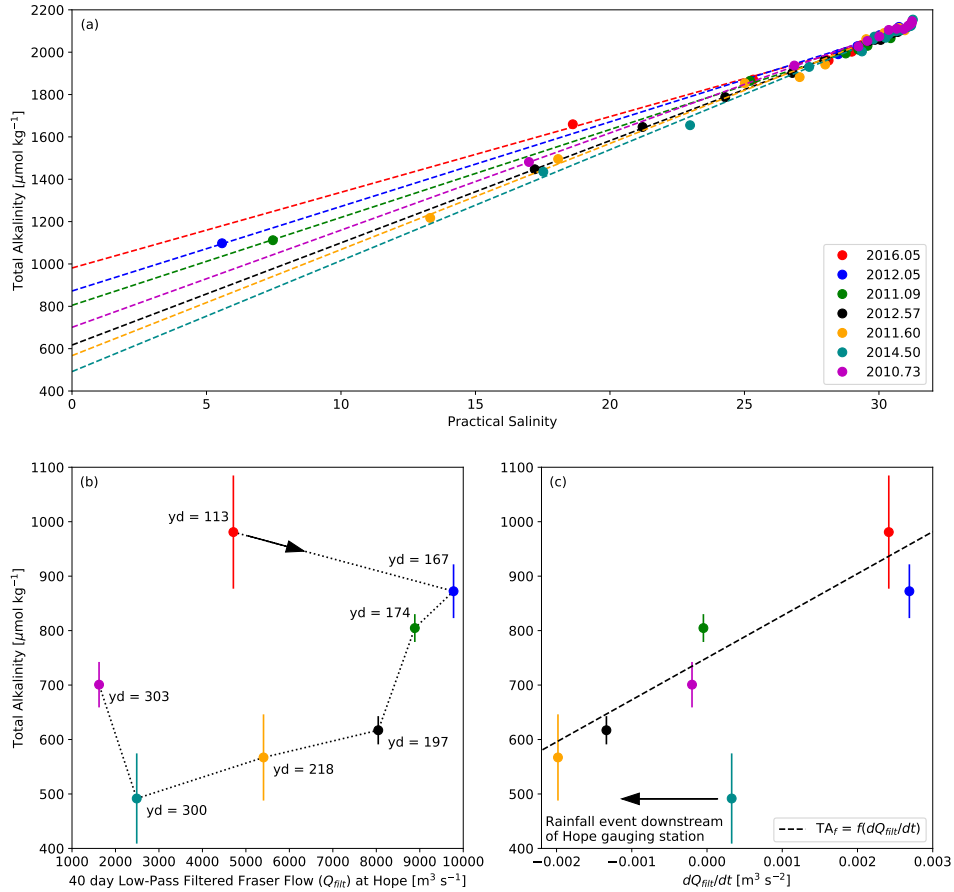
Figure 2. (a) Observed TA versus salinity (S) (circles) and linear regressions (dashed lines) from 7 Department of Fisheries and Oceans Canada (DFO) Strait of Georgia cruises in the Fraser River plume (Ianson et al. (2016), Table S1), (b) TA extrapolated to $S = 0$ versus low-pass filtered (40-day cutoff) Fraser River discharge (Q_{filt}) at Hope (circles) plotted in sequence of yearday (yd) as indicated by the dashed line and labels, and (c) TA extrapolated to $S = 0$ versus Q_{filt}/dt (circles) with the flow dependent freshwater TA parameterization used in this study (Eq. 1) overplotted (dashed line). Cruise ID numbers (legend) begin with the sampling year. Each cruise contains at least one datapoint at $S < 20$. Errorbars (b and c) are the 95% confidence intervals associated with the extrapolation to $S = 0$ using linear regression (a).
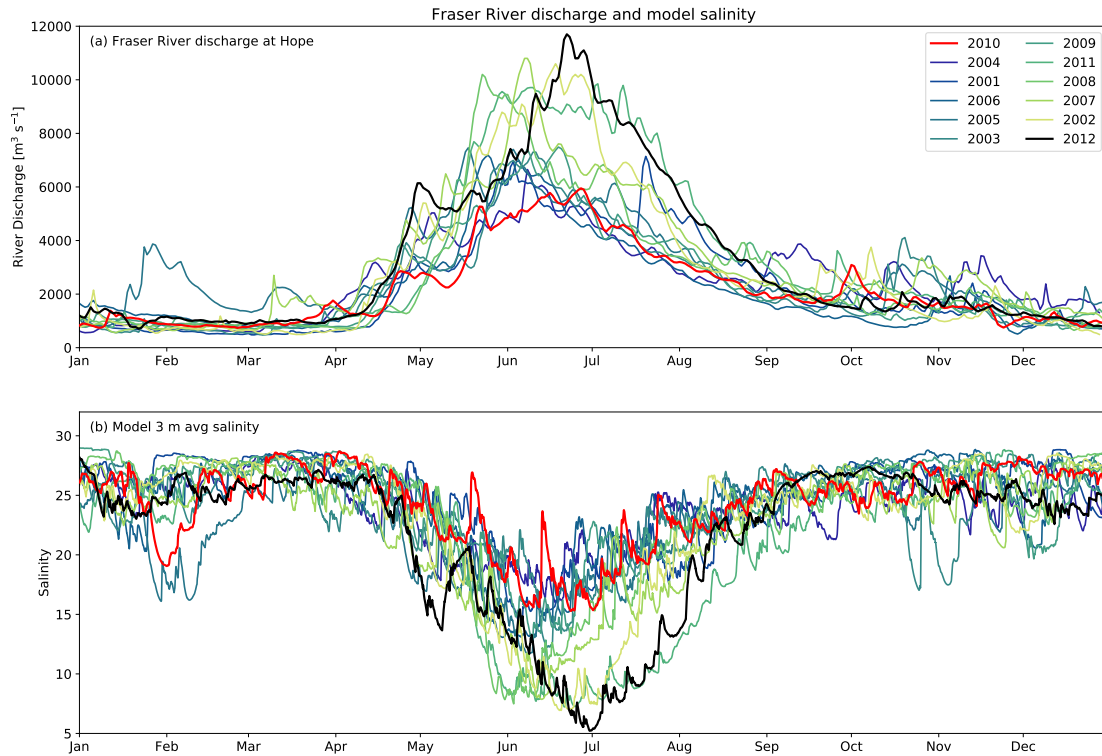
Figure 3. (a) Fraser River discharge at Hope versus yearday and (b) model top 3 m averaged salinity shown for each year in the 12 year period considered in this study. The Fraser River flow regime is characterized by a prominent summer freshet associated with summer glacial melt and smaller rainfall-dominated winter spikes. Model salinity reflects this overall pattern. Individual years are plotted in order of increasing freshet (peak) size. The smallest (2010) and largest (2012) flow years are highlighted in red and black, respectively.
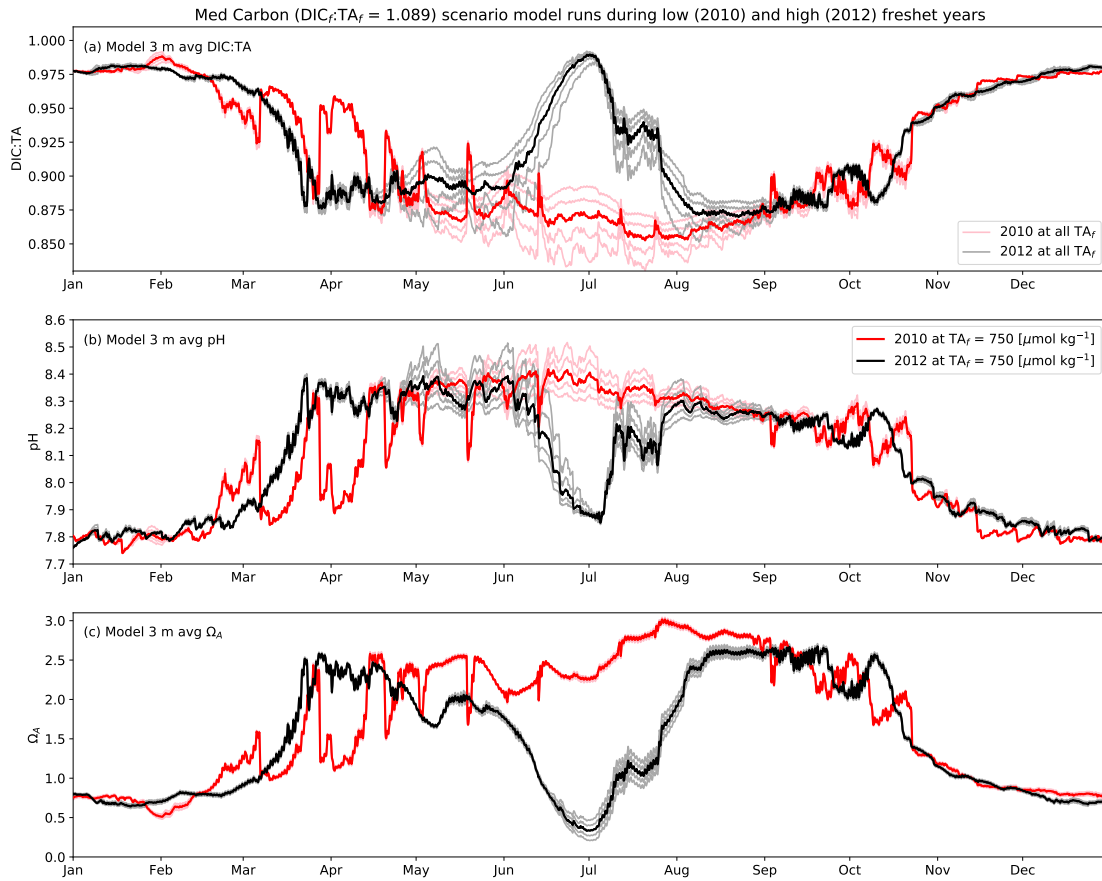
Figure 4. Timeseries of model top 3 m averaged (a) DIC:TA, (b) pH, and (c) Ω_A for all TA scenarios (Table 2) during 2010 (red/pink curves) and 2012 (black/gray) curves under the Med Carbon scenario (DIC_f:TA_f = 1.089), colors consistent with Fig. 3. The bold curves show model results at TA_f = 750 μmol kg^{-1} and the lighter curves show model results at all TA_f. All 3 quantities demonstrate a seasonal cycle consistent with biologically-driven DIC decreases in summer, increases in winter, and variations in spring associated with the spring bloom season. A strong mid-summer DIC increase is present in the 2012 results when river discharge is strong but absent in the 2010 results when river discharge is weaker.
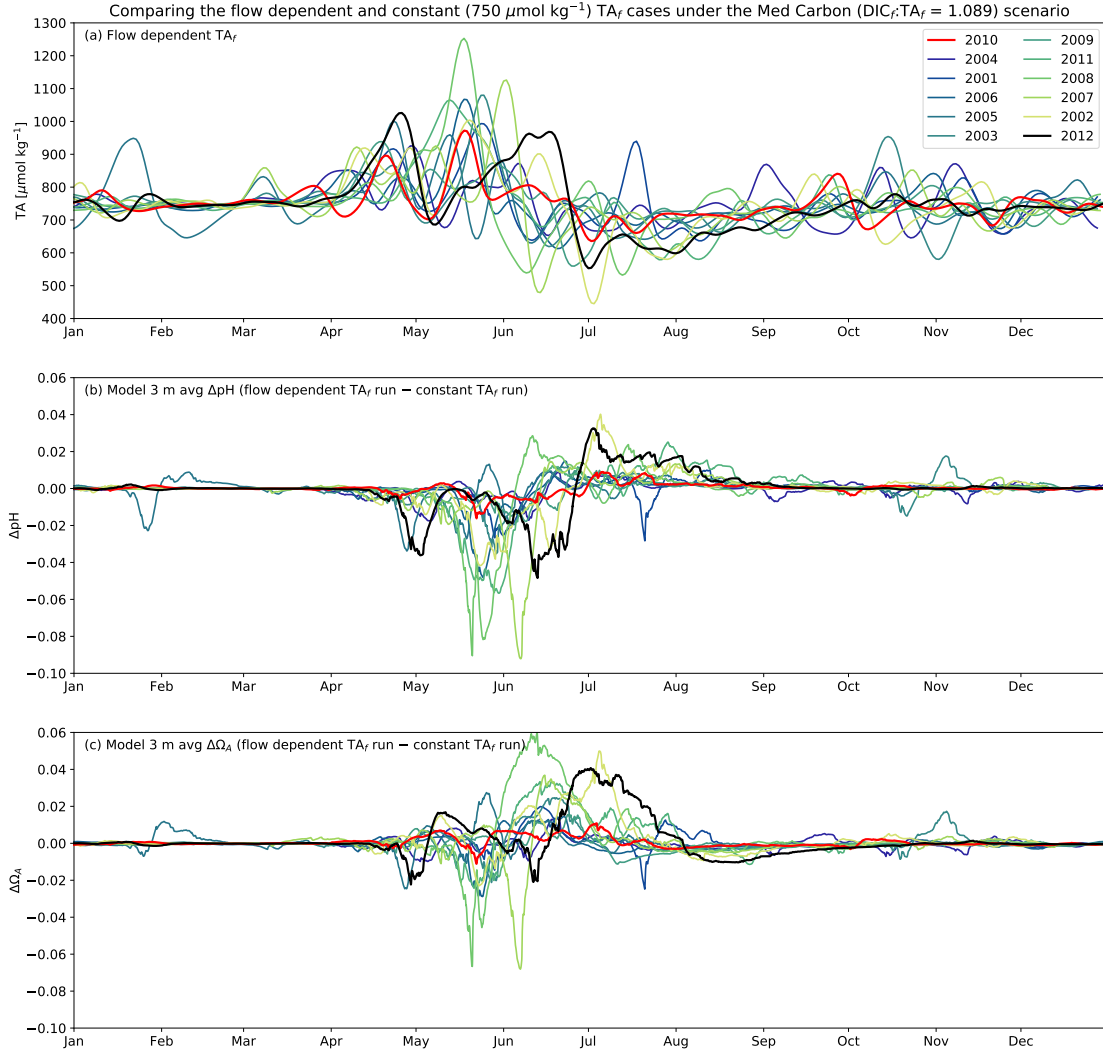
Figure 5. Results of the flow dependent TA$_f$ case for each year in the 12 year record: (a) The flow dependent TA$_f$ parameterization (Eq. 1), and (b and c) differences between flow dependent and constant (750 μmol kg^{-1}) TA$_f$ runs at (DIC:TA)$_f$ = 1.089 for (b) 3 m averaged pH and (c) 3 m averaged Ω_A. Years of record are plotted in order of increasing freshet size with the lowest (2010) and highest (2012) years highlighted in red and black, as in Fig. 3. Since flow dependence is proportional to dQ_{filt}/dt, the strongest effects surround the freshet generally with pH and Ω_A decreases prior to and increases after the freshet.

Figure 6. Salinity averaged (salinity < 20, summer) model (a-c) DIC:TA, (d-f) pH, and (g-i) Ω_A under the (left column) Low Carbon, (center column) Med Carbon, and (right column) High Carbon scenarios between all constant TA_f cases (horizontal axis) for each year in the full 12 year period (2001-2012). The salinity < 20 averages (circles) are plotted in order of increasing freshet size with the smallest (2010) and largest (2012) years highlighted as red and black stars, respectively, as in Fig. 3. Model DIC:TA (pH) generally increases (decreases) with increasing TA_f. Model Ω_A shares this trend under the High Carbon scenario but follows an opposite trend under the Low Carbon scenario.
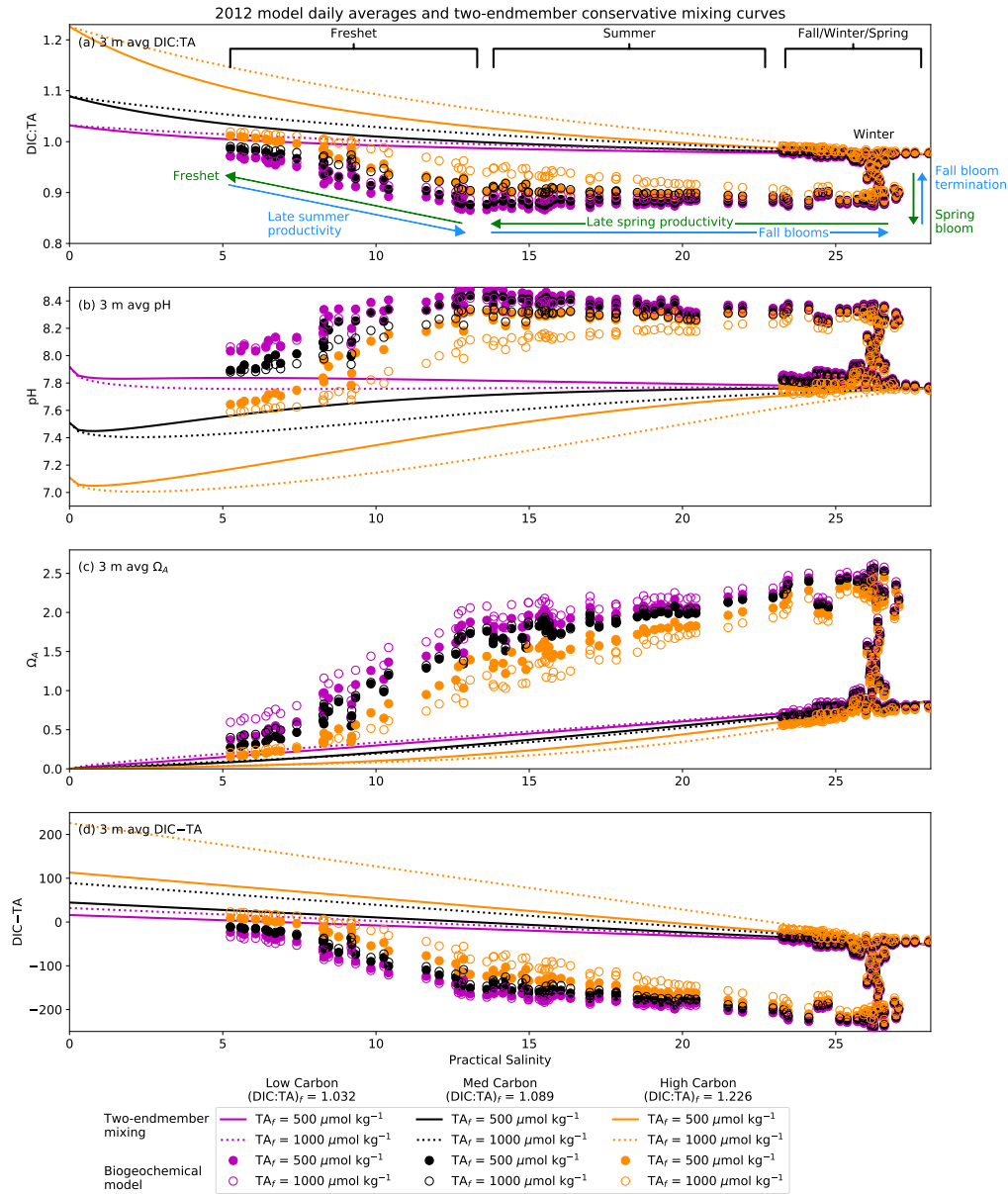
Figure 7. Daily model averages in salinity space during the largest freshet year (2012) of 3 m averaged (a) DIC:TA, (b) pH, (c) Ω_A, and (d) DIC−TA under the Low Carbon (DIC_f:TA_f = 1.032, magenta circles), Med Carbon (DIC_f:TA_f = 1.089, black circles), and High Carbon (DIC_f:TA_f = 1.226, orange circles) scenarios during 2 constant TA_f cases: TA_f = 500 μmol kg^{-1} (filled) and TA_f = 500 μmol kg^{-1} (open). Theoretical conservative mixing curves between the model freshwater and seawater endmembers (Table 1) calculated using CO2SYS are also shown (lines) for the corresponding DIC_f:TA_f and TA_f cases as indicated by color and line style, respectively (see legend). All runs demonstrate significant divergence from the theoretical curves during spring and summer while converging toward the freshwater endmember at low salinity during the freshet and toward the seawater endmember at high salinity during winter, as indicated by the annotations in (a). Differences between TA_f cases in the model are otherwise similar to the conservative mixing cases, however the effect of DIC_f:TA_f in the model is reduced relative to the mixing cases.
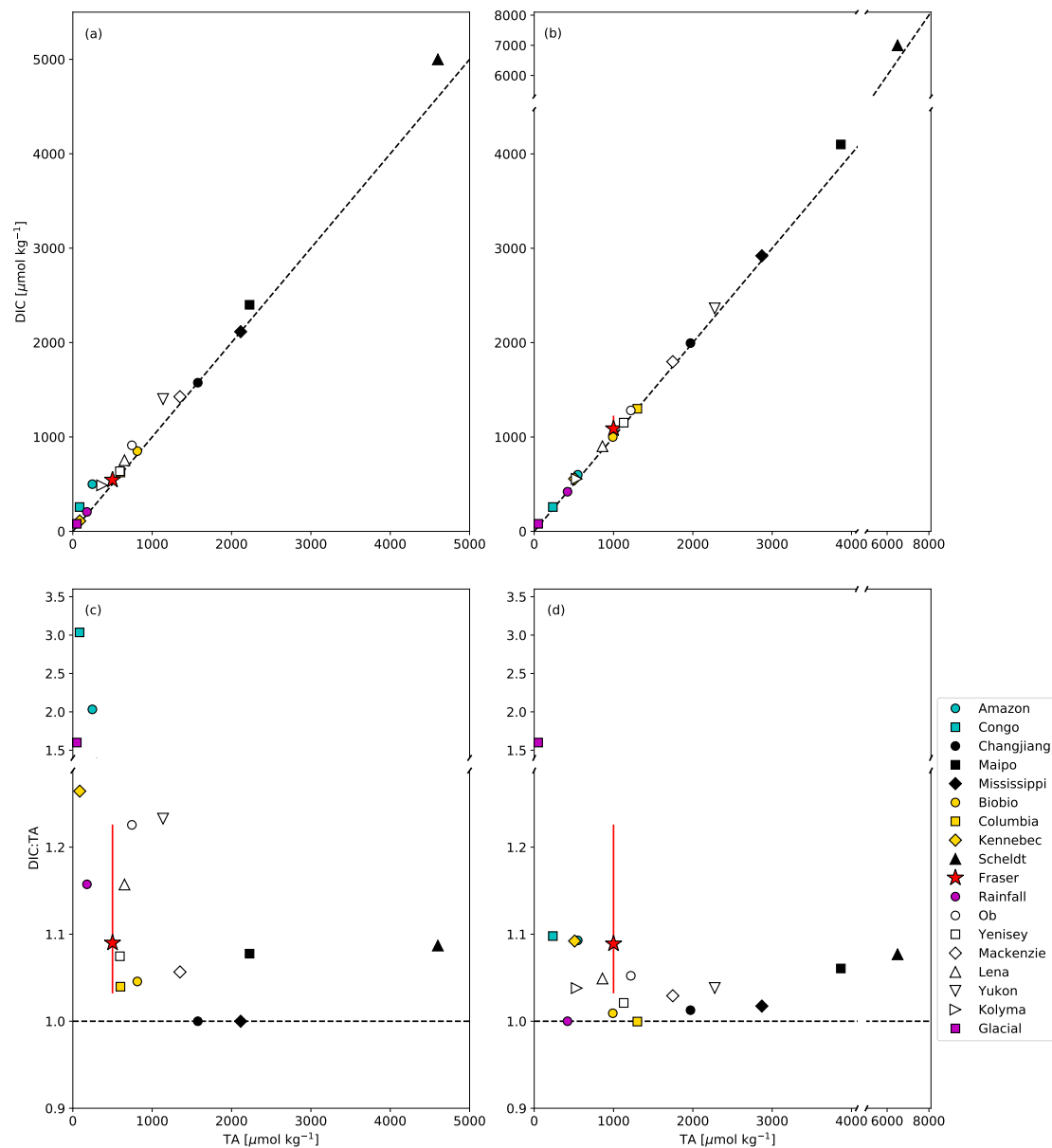
Figure 8. DIC and TA literature values for selected world rivers (Table S2) at the (a, c) low and (b, d) high ends of the reported ranges. The dashed lines are the DIC:TA 1:1 lines. The legend is in order of increasing latitude. Cyan symbols represent tropical watersheds, black symbols represent urbanized/polluted watersheds, yellow symbols represent temperate watersheds, magenta symbols represent watershed type proxies, and white symbols represent Arctic watersheds. The Fraser River DIC and TA endmembers used in this study (Table 2) are shown as a red star with errorbars to represent the range of DIC_f:TA_f scenarios. DIC data are unavailable for the Columbia River and thus calculated using reported TA and pCO_2 ranges. DIC and pCO_2 data are unavailable for the Arctic rivers and DIC is thus calculated from reported TA and pH ranges. TA data are unavailable for the Maipo and Biobio rivers and thus calculated using DIC and pCO_2. For most rivers, DIC:TA can be significantly greater than 1 (c, d) despite falling visually close to the 1:1 line (a, b). Uncertainty is not shown and not always reported.

Table 1. Model freshwater and seawater endmembers used to prescribe river fluxes and values at the 40 m boundary.

Endmember	Salinity [PSS-78]	Temperature [°C]	DIC [μmol kg^{-1}]	TA [μmol kg^{-1}]	Dissolved phosphorus[a] [μmol kg^{-1}]	Dissolved silica [μmol kg^{-1}]
Freshwater	0	10.9[b]	see Table 2	see Table 2	0.8	80.0
Seawater[c]	29.6	9.1	2020.0	2050.4	1.9	78.2

[a] Approximated from nitrate using the Redfield Ratio

[b] Midpoint of the model freshwater temperature range (2.5–19.3°C)

[c] Values presented are averages as seawater endmembers, except for nitrate and dissolved silica, are variable in the model

Table 2. Biogeochemical model freshwater endmember cases run for each year in the 2001-2012 year range.

ID	Name	$(DIC:TA)_f$	$pH_f^{(a)}$	TA_f (μeq kg^{-1})	DIC_f (μeq kg^{-1})	$DIC_f - TA_f$ (μeq kg^{-1})
LC1				250	258	8
LC2				500	516	16
LC3	Low			750	774	24
LC4	Carbon	1.032	7.8-8.0	1000	1032	32
LC5				1250	1290	40
LCV[b]				580-1015[c]	599-1047	19-32
MC1				250	272	22
MC2				500	544	44
MC3	Med			750	817	67
MC4	Carbon	1.089	7.4-7.6	1000	1089	89
MC5				1250	1361	111
MCV[b]				580-1015[c]	632-1105	52-90
HC1				250	306	56
HC2				500	613	113
HC3	High			750	920	170
HC4	Carbon	1.226	7.0-7.2	1000	1226	226
HC5				1250	1532	282
HCV[b]				580-1015[c]	711-1244	131-229

[a] pH_f range is across the model freshwater temperature range of 2.5-19.3°C

[b] Variable TA_f is given in Equation 1

[c] Variable TA_f parameter ranges are the 1st and 99th percentiles across the 12 year (2001-2012) dQ_{filt}/dt daily record